16th World Conference on Earthquake, 16WCEE 2017
Santiago Chile, January 9th to 13th 2017
Paper N° 1467 (Abstract ID)
Registration Code: S-K1461832539

ANALYTICAL STUDY OF THE EVALUATION PROCEDURE AND EFFECT WHEN BASE-ISOLATED BUILDING COLLIDES WITH RETAINING WALL

Soshi Nakamura[(1)], Takuya Suzuki[(1)], Takaki Tojo[(1)],
Shingo Asahara[(2)], Takuya Kinoshita[(2)] and Naohiro Nakamura[(3)]

[(1)] *Researcher, Research and Development Institute, Takenaka Corporation, nakamura.soushi@takenaka.co.jp*
[(2)] *Structural Designer, Structural Design Department, Takenaka Corporation, asahara.shingo@takenaka.co.jp*
[(3)] *Professor, Department of Architecture, Hiroshima University, naohiro3@hiroshima-u.ac.jp*

Abstract

In recent years, due to the effectiveness of reducing external force, many base-isolation buildings such as offices and hospitals have been constructed. However, in cases where a huge earthquake exceeds expected levels, there is a possibility that the deformation of the base-isolation layer will exceed the allowable displacement, causing the building to collide with the peripheral retaining wall.

When a building collides with a retaining wall, the physical properties of both the building and retaining wall will impact the behavior of the building before and after the collision. However, it is not clear what type or degree of impact will occur with regard to the behavior of the building. In addition, few studies have addressed the impact of the physical properties of the retaining wall. In this study, the authors evaluated the impact of the physical properties of the retaining wall on the behavior of the building.

First, the authors used a nonlinear finite element method (FEM) to create an analytical model that simulates a retaining wall of reinforced concrete and the back soil of the retaining wall, and then evaluated the load–displacement relationship by static analysis. Next, the authors used the sway–rocking model in which a nonlinear spring is used to evaluate the collision. Based on the load–displacement relationship, the authors performed a seismic response analysis. Finally, from the obtained results of the response analysis, the authors analyzed the impact and primary factors influencing the collision of the building with the retaining wall.

Based on our results, the authors can draw the following conclusions. First, with respect to the response state when a building collides with a retaining wall, the physical properties of the ground have a greater impact than those of the retaining wall. In addition, when the nonlinear characteristics were not considered as a collision spring, the authors found that an extremely high impact force is generated.

Keywords: 3-dimensional FEM, Nonlinear analysis, Retaining wall, Collision, Base-Isolated structure

1. Introduction

In recent years in Japan, there has been a risk of occurrence of massive earthquakes: one that would directly hit a metropolitan area or a Nankai Trough earthquake. As such, many basic-isolation buildings that can minimize the seismic force experienced by buildings have been constructed. Recently, to seismically retrofit traditional wooden buildings, there have been some cases in which buildings have been rebuilt as base-isolation buildings. In China, Italy, and New Zealand, base-isolation buildings are widespread and the production and study of basic isolators are ongoing. Basic-isolation buildings in Japan are mainly those in which the layer where a base isolator of rubber and oil damper is constructed (hereinafter referred to as the base-isolation layer) is placed at the bottom of the building to absorb energy due to deformation. This is known as foundation base isolation. Therefore, by predicting the maximum deformation of the base-isolation layer when an earthquake occurs and determining the movable range, also known as base-isolation clearance, buildings can be designed so that they do not collide with their peripheral retaining walls. However, when a massive earthquake that exceeds expectations occurs, there is a possibility that the magnitude of its input and the deformation of the base-isolation layer might exceed the limits of the design criteria. If the deformation of the base-isolation layer exceeds the criteria, the building will collide with the retaining wall.

Thus far, many research groups have investigated collision. Komaki et al. [1, 2] conducted a numerical analysis using a collision model in which a retaining wall was set as a cantilever beam and the back-facing ground was a linear spring. They found that when the height of the collision position is halved, the rigidity of the retaining wall is increased approximately 10-fold. On the other hand, in a study modeling the ground, the retaining wall, and the building in detail, Konno et al. [3] analyzed the collision of a building with a retaining wall using a 3D nonlinear FEM model, as well as the collision of the building/ground, by setting the collision experiment as a target. This suggests that numerical analysis is effective for evaluating base-isolation collisions. Okunaka et al. [4] also performed an analysis using a 3D nonlinear FEM model to determine the impact of two-way input and the response state in a building that was twisted and collided obliquely with the retaining wall due to variation in the rigidity of the base isolator.

Thus, studies on the collision of buildings with the retaining wall have employed various approaches. However, in cases involving a massive earthquake where a building collides with a retaining wall, it is considered that both the retaining wall and the ground would be nonlinearized. Therefore, there is a high possibility that the results of a linear evaluation of the retaining wall would greatly differ from the actual response. However, while conducting a nonlinear response analysis facilitates a most detailed examination by modeling all elements including the building, as done by Konnno and Okunaka, there is a possibility that the analysis load, such as the calculation time, could present another problem.

Accordingly, in this study, the authors propose a procedure for examining the nonlinear characteristics at the time of collision with a retaining wall while reducing the analysis load. Furthermore, by conducting a seismic response analysis in which the collision is taken into account, the authors examine the impact that differences in the retaining wall and the back soil have on the building response.

First, in Section 2, the authors create an analytical model in which the nonlinearities of the retaining wall and the ground are taken into account using the 3D FEM. In Section 3, the authors evaluate the load–displacement relationship of the retaining wall by static loading. Then, the authors set the concrete strength of the retaining wall and ground properties as parameters. In Section 4, the authors conduct a seismic response analysis using a mass system stress–release model that simulates a general base-isolation building. At this time, between the base-isolation layer and the ground, the authors add nonlinear spring elements that can reproduce the load–displacement relationship obtained by the FEM analysis conducted in Section 3. Finally, in Section 5, the authors compare the response results and evaluate the impact that the presence and absence of collision and differences in the physical properties have on the response.

2. Analysis Model

Here, the authors present details on the modeling of the retaining wall and the ground. For our analysis, the authors assumed a five-story reinforced-concrete planar structure of approximately 25 m × 60 m. On the base-

isolation layer in the lower section of the building, the authors located the base isolator consisting of a lead rubber bearing (LRB), a natural rubber bearing (RB), and an oil damper. In the periphery of the building, the authors assumed a retaining wall approximately 2.7 m high, with a base-isolation clearance of 65 cm between the building and the retaining wall. The authors also assumed the retaining wall to be constructed of reinforced concrete, with sand and clay as the back soil. In Section 4, the authors explain the modeling of the super structure.

2.1 Analysis Model of Retaining Wall

The retaining wall (2.7 m in height and 20 cm in thickness at the top) was constructed with reinforced concrete. The positional relationship between the retaining wall and the building is shown in Fig. 1, and the details of the reinforcement arrangement of the retaining wall are listed in Table 1.

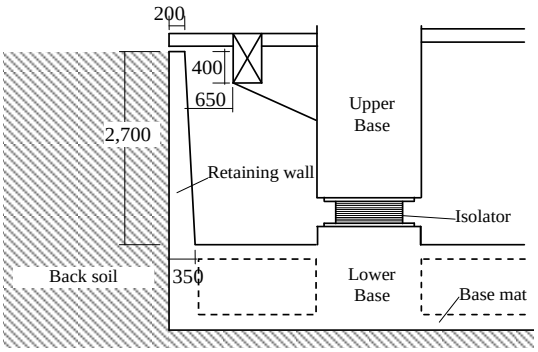

Fig. 1 – Positional Relationship between Retaining Wall and Building

Table 1 – Reinforcement Arrangement of Retaining Wall

	Back Soil Side	**Building Side**	
Vertical	D16@150	D16@200	
Horizontal	D13@200	D13@200	Upper Half
		D10@200	Lower Half

To account for the nonlinearity of the retaining wall section, the authors modeled the reinforced concrete and back soil using the 3D FEM. Setting the concrete and ground as solid elements; the authors modeled the reinforcing bar with a truss element. Fig. 2 shows the shape of the analytical model. The total number of nodes were 80,700 and the number of elements were 76,907 (of these, the number of solid elements was 74,448).

As boundary conditions, the authors fixed the bottom and YZ surfaces. With respect to the XZ surface, the authors fixed only its normal direction. The authors did not consider the friction surface of the boundary between the concrete and the ground.

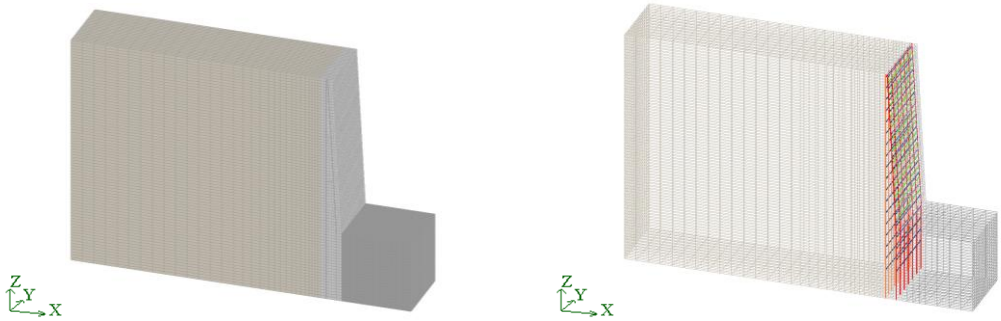

(a) Mesh Division (b) Reinforcement Arrangement

Fig. 2 – Analysis Model Shape

2.2 Nonlinear Characteristics of Concrete and Reinforcing Bar

The authors set the nonlinear characteristics of the reinforced concrete section using the method of Noguchi, et al. [5] as a reference. The authors set the concrete section as the model with a crack orthogonal in three directions. The uniaxial stress–strain characteristics are shown in Fig. 3. The authors set the stress–strain characteristics of the reinforcing bar as in the Menegotto–Pinto model. Tables 2 and 3 list the nonlinear material constants of the concrete and the reinforcing bar, respectively.

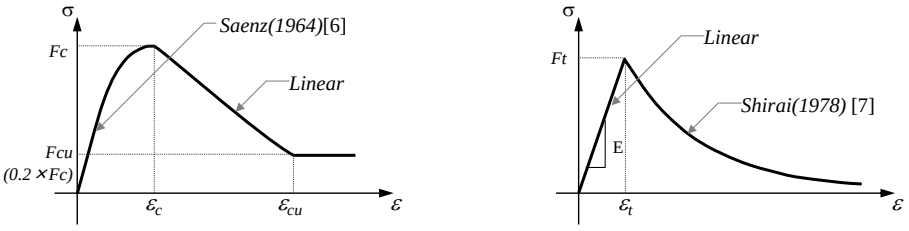

(a) Compression Direction (b) Tensile Direction

Fig. 3 – Nonlinear Characteristics of Concrete

Table 2 – Physical Properties of Concrete

Type	Compressive Strength F_c (N/mm^2)	Young Modulus E (N/mm^2)	Tensile Strength F_t (N/mm^2)	Poisson ratio	Density (t/m^3)	ε_c	ε_{cu}
Fc30	30.0	2.44E+4	2.08	0.20	2.24	0.0025	0.01
Fc60	60.0	3.07E+4	2.94				

Table 3 – Physical Properties of Reinforcing Bar

Rebar Type	Young Modulus (N/mm^2)	Poison ratio	Yield strength (N/mm^2)	Area (mm^2)
D16	2.06E+5	0.30	377	199
D13				127
D10				71.3

2.3 Nonlinear Characteristics of Ground

The authors assumed the back soil in the back of the retaining wall to be one of two types: sandy soil or clay. The authors determined the shear wave velocities of the sandy soil and clay to be of two types: Vs = 150 m/s where there is backfilled soil and Vs = 300 m/s where there is a certain level of the improved higher quality ground. Table 4 shows the material constants of the back soil. The authors used the Hardin–Dornevich model [8] to consider the nonlinear characteristics due to ground strain, as expressed in Equations (1) and (2) for sandy soil and clay, respectively. The parameters of the Hardin–Drnevich model used in our analysis are shown in Table 5, as referenced from the literature of the Architectural Institute of Japan. Fig. 4 shows the dynamic deformation characteristics.

$$\frac{G}{G_0} = \frac{1}{1+\dfrac{\gamma}{\gamma_{0.5}}} \tag{1}$$

$$h = h_{\max}\left(1-\frac{G}{G_0}\right) \tag{2}$$

where G/G_0 = Rigidity lowering rate; $\gamma_{0.5}$ = Reference strain; and h_{max} = Initial damping.

Table 4 – Ground Properties of Back Soil

Type	Vs (m/s)	Shear Modulus (N/mm^2)	Density (t/m^3)	Poisson ratio
Vs150	150	3.60E+4	1.6	0.45
Vs300	300	1.44E+5		

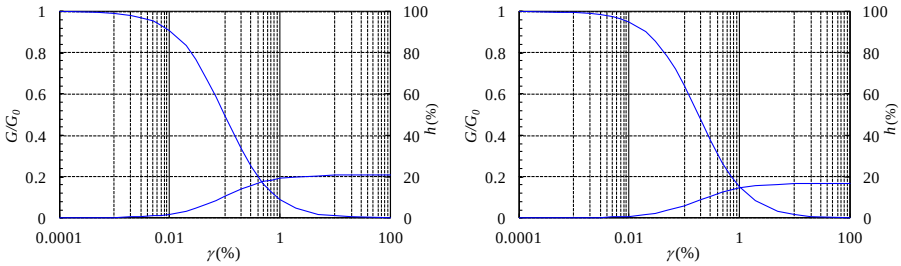

(a) Sandy (b) Clay

Fig 4 – Dynamic Nonlinear Characteristics

Table 5 – Parameter of Hardin–Drnevich Model

	$\gamma_{0.5}$(%)	h_{max}(%)
Sandy	0.10	21
Clay	0.18	17

3. Static Analysis of Retaining Wall

3.1 Analysis Cases

In the static analysis, the authors uniformly applied forced displacement with a range of 40 cm from the top of the retaining wall as the area where the building collides. To evaluate the load–displacement relationship from loading to unloading after the forced displacement reaches maximum displacement, the authors reset the displacement to 0. The forced displacement was carried out in two ways whereby the maximum deformation becomes 1.0 cm in the 2,000STEP and 0.5 cm in the 1,000STEP. Fig. 5 shows the time history of the forced displacement. In the analysis, the authors set the Vs value of the ground, concrete strength, and maximum deformation at the top as parameters. A list of the static analysis cases is shown in Table 6.

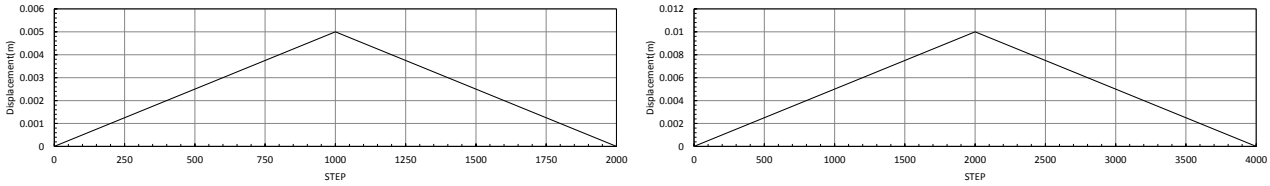

(a) Maximum deformation = 5 mm (b) Maximum deformation = 10 mm

Fig. 5 – Time History of Forced Displacement

Table 6 – Static Analysis Cases

Sandy Soil			
Case	**Vs (m/s)**	**Fc (N/mm^2)**	**Deformation (mm)**
S-1	150	30	5.0
S-2			10
S-3		60	5.0
S-4			10
S-5	300	30	5.0
S-6			10
S-7		60	5.0
S-8			10

Clay Soil			
Case	**Vs (m/s)**	**Fc (N/mm^2)**	**Deformation (mm)**
C-1	150	30	5.0
C-2			10
C-3		60	5.0
C-4			10
C-5	300	30	5.0
C-6			10
C-7		60	5.0
C-8			10

3.2 Static Analysis Results (Load–Displacement Relationship)

Fig. 6 shows the load–displacement relationship obtained by static analysis. Here, the horizontal axis is the forced displacement, which is provided with the loading section, and the vertical axis is the total reaction force of all the nodes within the range of the loading section. Table 7 lists the maximum proof stress (at deformations of 5.0 and 10 mm) for each case and the initial rigidities. From Fig. 6 and Table 7, with respect to the impact of

the maximum proof stress and the initial rigidity, the authors see that the rigidity of the back soil has a greater impact than the compressive strength of the retaining wall.

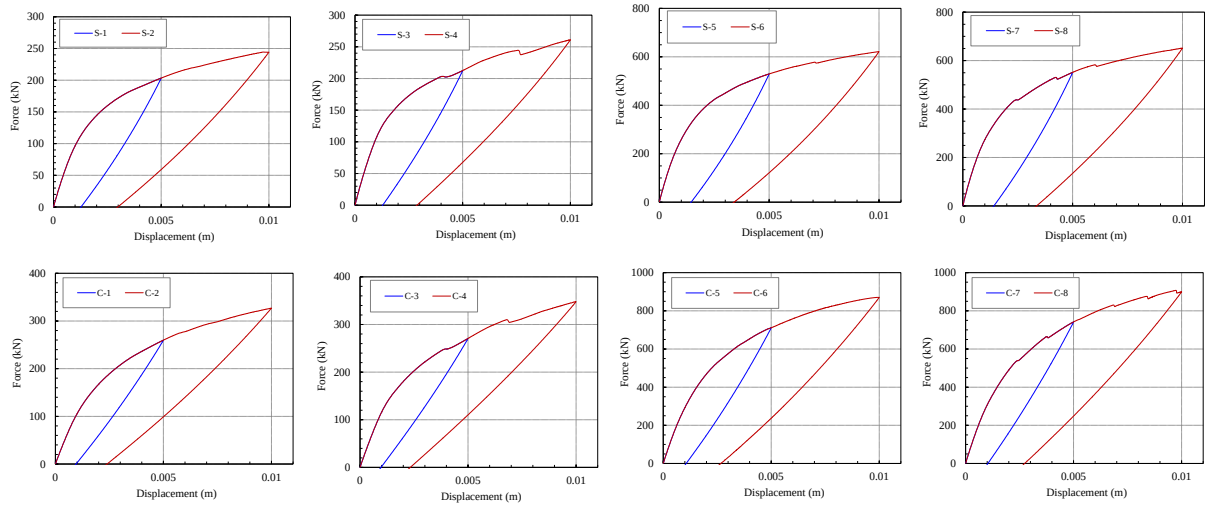

Fig. 6 – Load–Deformation Relationship by Static Analysis

Table 7 – Maximum Proof Stress and Initial Rigidity by Static Analysis

Case	Vs (m/s)	Fc (N/mm^2)	$F_{0.5}$ (kN)	$F_{1.0}$ (kN)	K_0 (kN/m)
S-1 S-2	150	30	203	244	1.24E5
S-3 S-4		60	213	261	1.34E5
S-5 S-6	300	30	530	622	3.59E5
S-7 S-8		60	552	652	3.73E5

Case	Vs (m/s)	Fc (N/mm^2)	$F_{0.5}$ (kN)	$F_{1.0}$ (kN)	K_0 (kN/m)
C-1 C-2	150	30	260	327	1.24E5
C-3 C-4		60	271	348	1.34E5
C-5 C-6	300	30	711	871	3.59E5
C-7 C-8		60	742	907	3.73E5

3.3 Conversion to Spring Element

Next, the authors converted the load–deformation relationship obtained above to a nonlinear spring element for use in the seismic response analysis described in Section 4. The shape of the nonlinear spring used in the collision evaluation is shown in Fig. 7. When the relative displacement of the spring reaches a base-isolation clearance of δc, collision occurs; prior to this an extremely low rigidity K_1 is set. Moreover, in the response analysis described in Section 4, the authors analyzed the nonlinear elasticity spring while ignoring nonlinearity after the collision.

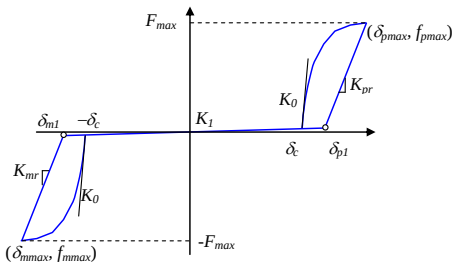

Fig. 7 – Nonlinear Spring for Collision Evaluation

After collision, the authors set the path to fit to the load–deformation relationship shown in Fig. 6. To load the path after collision, fitting was performed using the hyperbolic curve model, as shown in Equation (3):

$$K_r = K_0 \cdot \frac{1}{1+\frac{\delta}{\delta_{50}}} \tag{3}$$

where K_r = Rigidity at the time of loading; K_0 = Initial inclination (rigidity of loading of 1STEP); $\delta_{50} = F_{max}/K_0$; F_{max} = Strength of the hyperbolic curve; and δ = Relative displacement of spring–clearance δ_c

The authors set the unloading path after collision as linear based on the unloading rigidity K_{pr} obtained by Equations (4) and (5) below. Because the value of K_{pr} varies with the unloading position, it was possible to obtain this value by determining the displacement δ_r at the time of unloading. The authors obtained coefficient b in Equation (4) and coefficients A and C in Equation (5) using the least-squares method in order to minimize the difference between the unloading inclinations $K_{p0.5}$ and $K_{p1.0}$ obtained from Fig. 6. The parameters of F_{max}, $K_{p0.5}$, and $K_{p1.0}$ that the authors set for each examination condition are listed in Table 8.

$$K_{pr} = a \cdot \left(\frac{F_{\max}}{\delta_r} \right)^b \tag{4}$$

$$a = A \cdot \left(\frac{V_S}{150} \right)^C \tag{5}$$

where δ_r = Displacement at the time of unloading; Vs = Shear wave velocity of back soil; b = 0.553; A = 0.00096; and C = -0.75

In the unloading case that exceeded the point δ_{p1}, at the intersection of the straight line by K_1 before collision and the straight line of the unloading inclination, the authors set this value to return to a skeleton value in the linear state before collision. The authors explain the behavior at the time of the collision again with using the behavior of positive side as an example. The authors defined it as being in the linear state by rigidity K_1 until exceeding δ_{p1}, in the linear state by rigidity K_{pr} until δ_{pmax} after exceeding δ_{p1}, and after exceeding δ_{pmax}, it follows the path that shifts to the skeleton curve of the hyperbolic model. In Fig. 8, the load–displacement relationship obtained by the analysis is shown with superposing on the loading and unloading paths obtained from the approximation Equations (3)–(5). By these approximation equations, the authors can satisfactorily reproduce the load–displacement relationship obtained by the analysis.

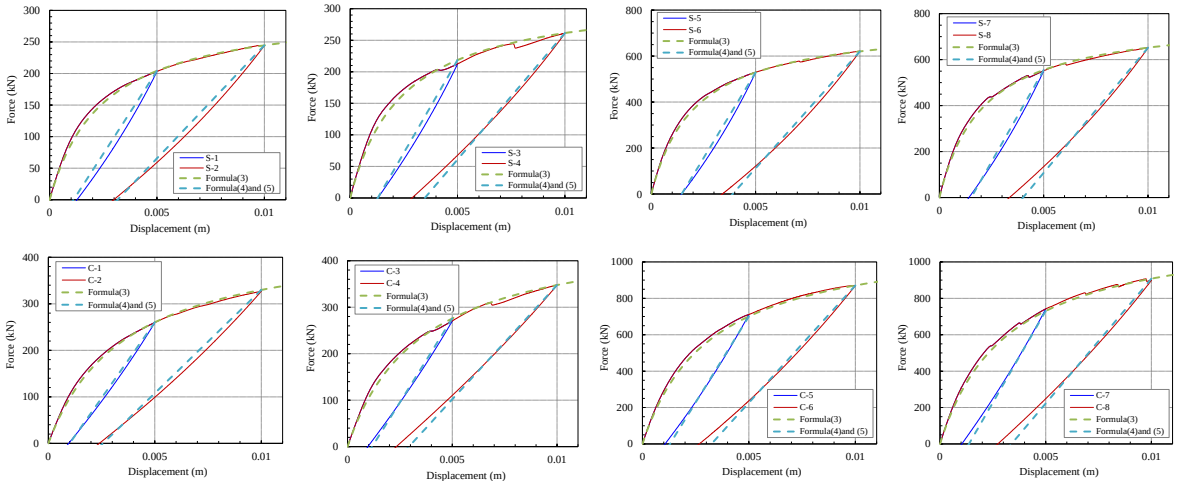

Fig. 8 – Fitting via Load–Displacement Relationship by FEM and Approximation Equations

4. Seismic Response Analysis

In this section, the authors describe the seismic response analysis model of the building, the input seismic motion, and the analysis conditions.

4.1 Analysis Model

As mentioned in Section 2, in this study, the authors examined a five-story reinforced-concrete structure and set the specifications for the analysis model following Tojo et al [9]. The authors set the analysis model to be multi-degrees-of-freedom uniaxial, as shown in Fig. 9, and modeled the base-isolation layer as a horizontal direction spring. The authors determined the lower end of the base-isolation layer to be fixed, and to the first floor section, the authors added the nonlinear spring at the point of collision with the retaining wall modeled in the previous chapter. The authors modeled each story of the upper structure as a linear shear spring, and the specifications of the building are shown in Table 9.

With respect to the basic isolator, the authors assumed there were a total of 40 base-isolation rubbers (RB and LRB) and two oil dampers for each direction. The authors established the restoring force characteristics of the base-isolation layer by setting RB and the oil dampers as linear models and the LRB as a bilinear model. The authors did not take the hardening characteristics of the rubber into consideration. The specifications of the assumed base isolator are listed in Table 10 and its dynamic characteristics are shown in Fig. 10. The results of the eigenvalue analysis revealed that the cycle in the fixed conditions of the base-isolation layer was 0.62 s (f = 1.61Hz), and the equivalent cycle in the case when the strain of the base-isolation layer reached 300% was 3.38 s (f = 0.30Hz). About the damping, the authors set the Rayleigh's damping as the damping type of the analysis model, and set 0.03 as damping ratio for the above two frequencies. The authors also assumed that the collision between the retaining wall and the building occurred simultaneously on the entire surface of the shorter sides.

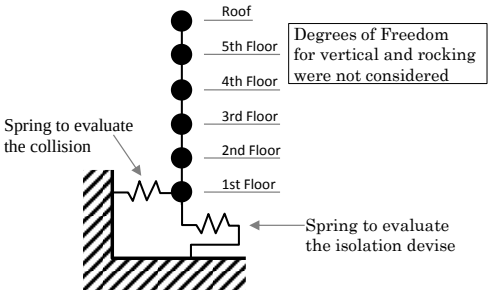

Fig. 9 – Response Analysis Model

Table 9 – Specifications of Building Model

Floor	Hight(m)	Mass(t)	Shear Stiffness(kN/m)
roof	20.0	500	-
5th	16.0	1,800	3.0×10^5
4th	12.0	1,800	6.0×10^5
3rd	8.0	1,800	9.0×10^5
2nd	4.0	1,800	1.2×10^6
1st	0.0	2,000	1.6×10^6

Table 10 – Specifications of Base Isolator

Type		K_1 (KN/m)	K_2 (KN/m)	Qy (KN)	quantity
RB	1	795	-	-	12
	2	910	-	-	17
LRB		11,120	855	174	11
Oil Damper		C = 2,500kNs/m			2

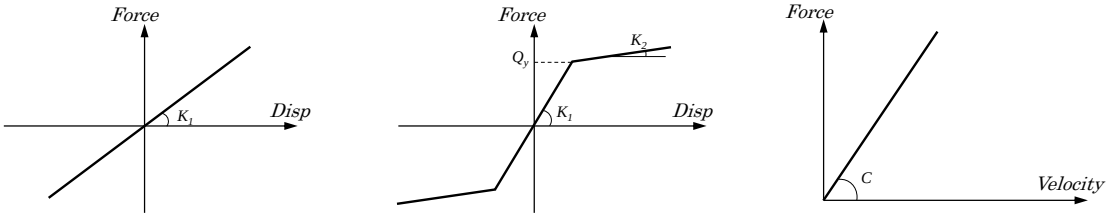

(a) RB (b) LRB (c) Oil-Damper

Fig. 10 – Dynamic Characteristics of Base Isolator

4.2 Input Seismic Motion and Analysis Case

For the analysis, the authors used the input seismic motion by doubling the long-period ground motion that was created by the assumption of Nankai Trough 4 consolidated earthquakes as released by the Building Research Institute [10]. The maximum acceleration was approximately 1,000 gal and the duration time was 300 s. Fig. 11 shows the acceleration time history and acceleration response spectrum (h = 5%) of the input seismic motion (ground surface). Furthermore, for the analysis, the authors used the Newmark-β method (β = 1/4) with an analysis time increment of 0.001 s.

The implemented response analysis case is shown in Table 10. For comparison, the authors also analyzed the case in which no collision was considered and that in which the spring after collision is set as a linear spring. With respect to the rigidity of the linear spring, the authors used the initial rigidity K_0 obtained in the analysis case S-1 in Table 7.

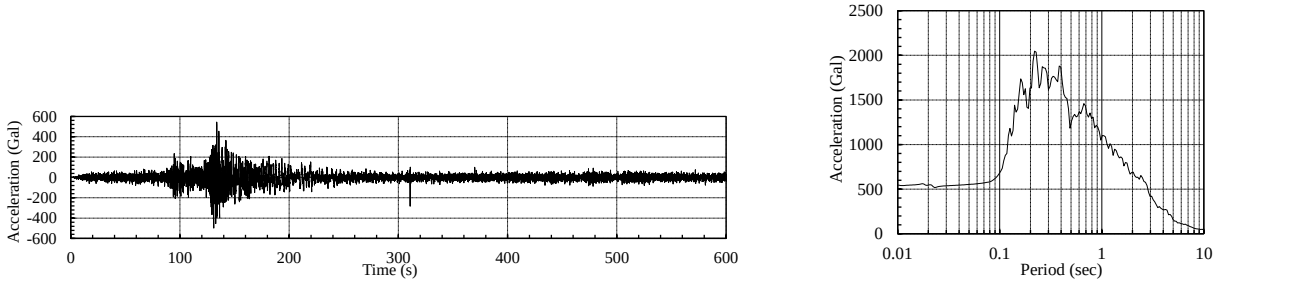

(a) Acceleration Time History (b) Acceleration Response Spectrum (h = 5%)

Fig. 11 – Input Earthquake Motion

Table 11 – Conditions for Response Analysis Case and Ground Spring

Case	Vs (m/s)	Fc (N/mm^2)	Soil Type
Vs150-Fc30-S	150	30	Sandy
Vs150-Fc30-C			Clay
Vs150-Fc60-S		60	Sandy
Vs150-Fc60-C			Clay
Vs300-Fc30-S	300	30	Sandy
Vs300-Fc30-C			Clay
Vs300-Fc60-S		60	Sandy
Vs300-Fc60-C			Clay
No-Spring	-		
Linear-Spring	150	Fc30	Sandy

5. Response Analysis Results

Fig. 12 shows the height directional distributions of the maximum response displacements, accelerations, and shearing forces. In addition, for comparison, these figures show the response results for cases in which the collision spring is set as a linear spring and those of the non-collision case.

The response acceleration and shearing force of the case in which the collision is modeled as a nonlinear spring were between the response values of the non-collision and linear collision spring cases.

With respect to the nonlinear and linear collision spring cases, in the collision where the maximum impact force occurs, Fig. 13 shows the time history waveform of the impact force that the building received from the retaining wall and the acceleration time history of the material point of 1st floor. The authors can see that in both cases, at the time when the impact force due to collision is generated, a large peak occurs in the acceleration time

history. In the case of the linear collision spring, an extremely large impact force occurs, which is 5–10 times greater than that of the nonlinear collision spring case. Moreover, the maximum value of acceleration immediately after collision exceeds 3,000 gal. Thus, in the case where collision is evaluated as a linear spring, although the evaluation is on the safe side, it can be said that the acceleration and shear force are significantly overestimated.

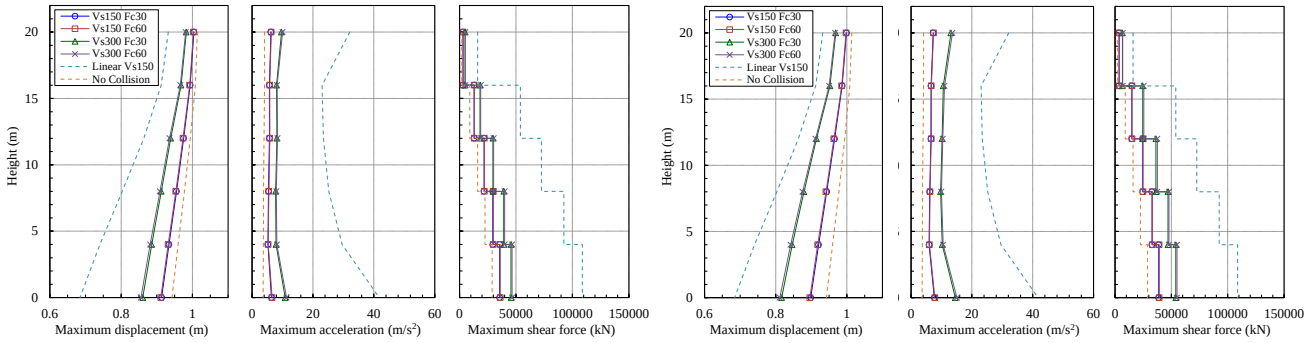

(a) Soil Classification: Sand (b) Soil Classification: Clay

Fig. 12 – Maximum Response Value Distribution

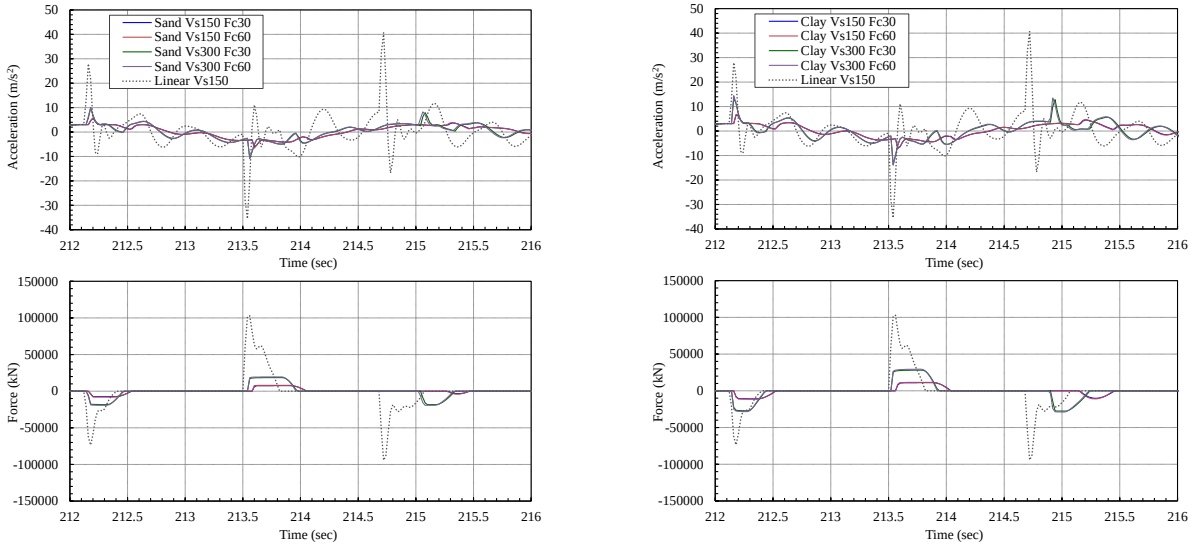

(a) Soil Classification: Sand (b) Soil Classification: Clay

Fig. 13 – Comparison of Impact Force and Acceleration Time History

Next, in Fig. 14, where the horizontal axis is the compressive strength; the shear wave velocity of the ground and ground classification, the maximum acceleration, the shear force, and impact force of the material point of 1st floor for each case are plotted on the vertical axis, respectively.

As shown in the figures, there is little increase in the response value from an increase in the compressive strength of the retaining wall, from 30 to 60 N/mm^2, and little impact of the concrete strength of the retaining wall on the response. On the other hand, as the shear wave velocity of the back soil increases from 150 to 300 m/s, the response shear force increases by over 1.3 times and the impact force by over 2.4 times; from this, the authors can conclude that the rigidity of the back soil has a significant impact on the building response.

Next, a comparison of the sand and clay grounds reveals that clay ground has the larger shear force with acceleration values of approximately 1.3 times and 1.5 greater impact force. As such, the authors can conclude that similar to the rigidity of the back soil, the ground classification also has a significant impact on the building response.

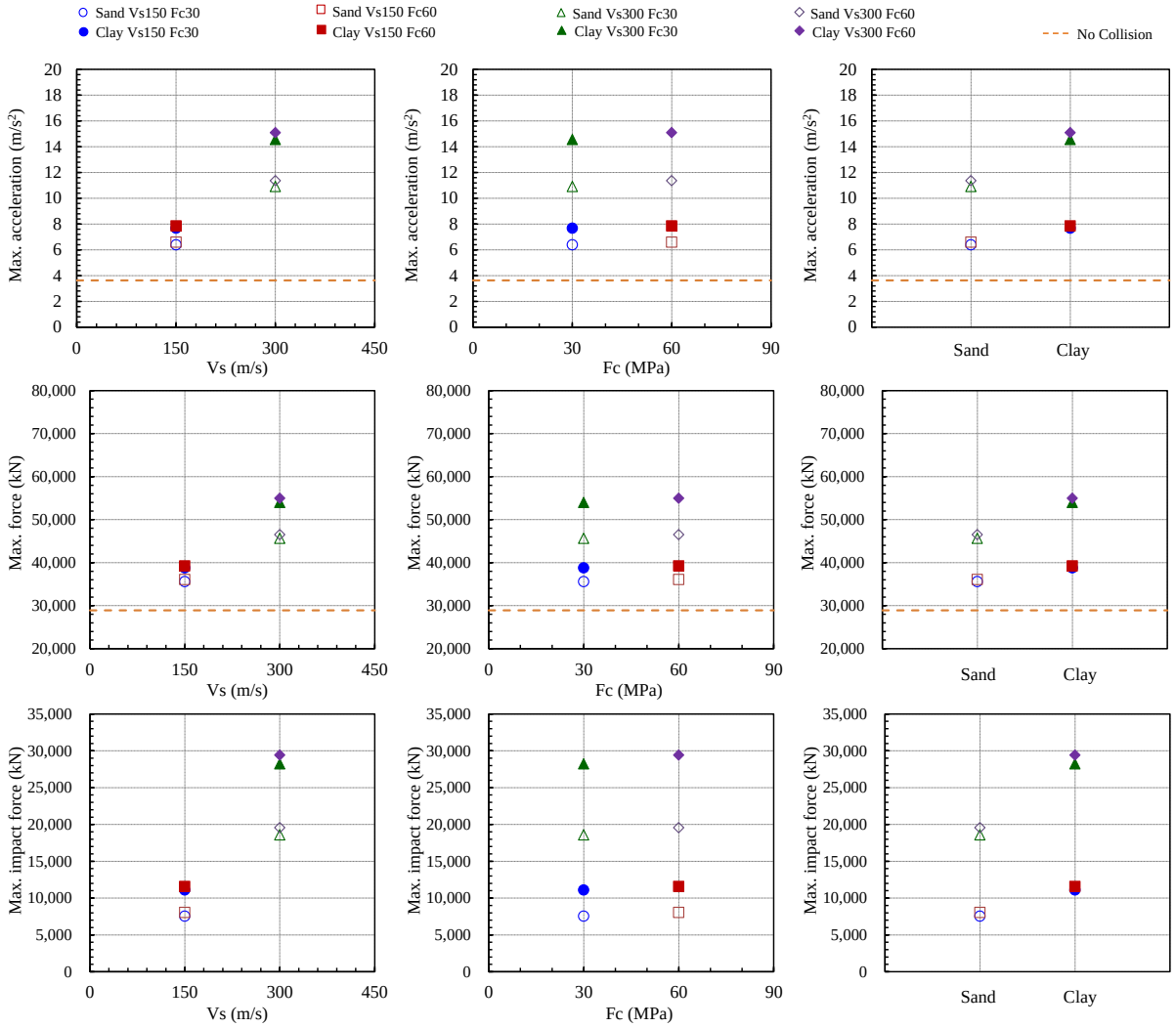

Fig.14 – Relationship among Compressive Strength of Retaining Wall, Shear Wave Velocity of Ground, Ground Classification, and Response of 1st Floor

6. Conclusion

In this study, the authors used static analysis with a nonlinear 3D FEM model and a dynamic analysis with a lumped mass model to examine the impact of the physical properties of the retaining wall on the response of a building when it collides with the retaining wall. Based on our results, the authors were able to draw the following conclusions:

- From our nonlinear 3D FEM analysis of the load–displacement relationship at the time of collision with the retaining wall, the obtained results indicate that the concrete strength of the retaining wall has only a small impact on the initial rigidity and unloading inclination in the load–displacement relationship, while the rigidity of the ground at the back of the retaining wall has a large impact.
- The response analysis results of the case in which the authors evaluated the collision as a nonlinear collision spring, as proposed in this study, were between the results of the noncollision and linear collision cases and did not depend on the concrete strength or ground physical properties. However, in the case in which the collision was evaluated as a linear spring, results show the acceleration and shear force to be significantly overestimated.

- As a result of our comparison of the impact that the concrete strength, shear force wave velocity of the ground, and ground classification have on the response of 1F, the authors found that the impact on the ground side has a larger impact relative to the rigidity of the retaining wall itself. Note that the impact of the shear wave velocity was particularly large.

In future, by increasing the number of parametric examination cases by 3D FEM analysis, the authors will propose an evaluation system whereby the retaining wall collision spring can be calculated based on the setting conditions. Moreover, the authors will compare our results with those of full-scale collision experiments to verify the validity of our proposed collision spring evaluation procedure.

7. References

[1] Komaki J, Miwada G, Takiyama N, Onishi Y, Hayashi Y (2012): Designing Evaluation Method of Retaining Wall Stiffness -Part 2- Construction of the Evaluation Method. *Summaries of Technical Papers of Annual Meeting*, AIJ, Structure II, 261-262 (In Japanese)

[2] Miwada G, Komaki J, Onishi Y, Hayashi Y (2012): Designing Evaluation Method of Retaining Wall Stiffness -Part 3- Comparison Evaluation with Experimental Result. *Summaries of Technical Papers of Annual Meeting*, AIJ, Structure II, 263-264 (In Japanese)

[3] Konno Y, Kanai Y, Manabe Y, Niwa K, Tsubota H, Kasai Y (2012): Seismic Response Analysis Considering Collision into Retaining Wall using 3-Dimensional Nonlinear FEM -Part 1- Basic Behavior. *AIJ Kanto Chapter Research Meeting*, **Vol.1**, 253-256 (In Japanese)

[4] Okunaka R, Miyamoto Y, Kashiwa H, Watanabe S (2000): Study on Response of Base-Isolation Building in Oblique Collision with Retaining Wall, *Journal of Structural and Construction Engineering*, AIJ, **Vol.79**, No.76, 1763-1771 (In Japanese)

[5] Noguchi H, Kashiwazaki T, Miura K (2006): Finite Element Analysis of Reinforced Concrete Joints Subjected to Multi-Axial Loading, TTC Hsu Sympo., ACI, SP-265, pp223-244

[6] Saenz L.P. (1964), Discussion of Equation for the Stress-Strain Curve of Concrete, *Proc. of ACI*, **Vol.61**, No.9, 1229-1235

[7] Sato T, Shirai N (1978): Elastic-Plastic Behavior of RC Shear Walls, *Summaries of Technical Papers of Annual Meeting*, AIJ, C-2, 1615-1618 (In Japanese)

[8] Hardin B.O., Drnevich V.P. (1972):Shear Modulus and Damping in Soils: Design Equations and Curves, *Proc. of ASCE*, SM7, 667-692

[9] Tojo T, Nakamura N, Kinoshita T, Suzuki T (2012): Analytical Study on Impulsive Force between Base-Isolated Building and Retaining Wall, *Summaries of Technical Papers of Annual Meeting*, Structure II, 355-356 (In Japanese)

[10] Building Research Institute (2013): Study on Long-Period Ground Motions and Responses of Super-High-Rise Buildings ETC. –Evaluations of Responses of Super-High-Rise and Seismically-Isolated Buildings under the Hypothetical Maximum Level Earthquake in Nankai Trough Region-, *Building Research Data*, No.147 (In Japanese)